ANNALS OF GEOPHYSICS, 67, 3, S323, 2024; doi:10.4401/9049
OPEN ACCESS

Dependence of horizontal PGA prediction on site conditions at critically short hypocentral distances: An analysis based on Japanese strong motion data

Najmeh Masoumi[1], Hossein Sadeghi[*,2], Majid Sarmad[3]

(1) Ferdowsi University of Mashhad, Earthquake Research Center, Mashhad, Iran
(2) Ferdowsi University of Mashhad, Department of Geology, Mashhad, Iran
(3) Ferdowsi University of Mashhad, Department of Statistics, Mashhad, Iran

Article history: received November 25, 2023; accepted July 8, 2024

Abstract

A fundamental element in seismic hazard assessment studies is the prediction of maximum values of ground accelerations. This is achieved through an attenuation relationship, also known as the ground motion prediction equation (GMPE). Seismic design of structures generally assumes the occurrence of a large earthquake on a nearby fault. The predictions from the GMPE are linked to the magnitude, distance, and local site conditions. Critical near-fault ground motions have unique characteristics such as magnitude saturation and distance saturation. To investigate the impact of local site conditions in the near-fault region, we analyzed the attenuation relations using the accelerations recorded in Japan by the Kiban Kyoshin network (KiK-net) from 2000 to 2023. All events with a magnitude equal to or greater than 5.5, and with focal depth and epicentral distance less than 20 km, were considered. In this study, the hypocentral distance ranges from 5 to 23 km. Ordinary least squares regression analysis was conducted for the maximum horizontal vector of ground accelerations. The attenuation relation coefficients for horizontal vector peak ground acceleration were estimated using an effective distance and saturation effect. An additional independent term, the average shear wave velocity of the soil to a depth of 30 meters below the ground surface, and more cost-effective shallower depths were included in the regression model. The analysis revealed that the site condition is statistically non-significant at very short hypocentral distances of less than 23 kilometers.

Keywords: Near Fault; Ground Motion Prediction; Site Effect; Peak Ground Acceleration; KiK-net

1. Introduction

Although harmful earthquakes cannot be avoided, the risk associated with this natural phenomenon can be significantly reduced through proper hazard analysis. Estimating strong ground shaking from scenario earthquakes is fundamental to seismic hazard analysis. This is achieved through a relationship called Ground Motion Prediction Equation (GMPE) or attenuation relationship.

To develop attenuation relations, various theoretical and empirical methods have been introduced. In general, theoretical approaches simulate ground motions by considering information about the earthquake source, wave propagation, and local site conditions, while empirical methods analyze observed seismic data to fit a model function that estimates ground shaking. An empirical prediction model determines the amplitude of ground motion, such as peak ground acceleration, based on known input parameters. Input parameters typically include magnitude, source-to-site distance (e.g., epicentral distance, hypocentral distance, rupture distance), and site conditions (e.g., soil class, shear wave velocity profile).

Earthquake prediction for the seismic design of structures usually assumes a large earthquake in adjacent faults. The ground motion during an earthquake could be substantially different in an area near to and far from the earthquake source. The earthquakes in the area close to the causative faults generally have higher destructive effects on structures. Catastrophic earthquakes such as the Northridge (1994) earthquakes in California, Kobe (1995) in Japan, Izmit (1999) in Turkey, Chichi (1999) in Taiwan, and Bam (2003) in Iran were located near cities and populated areas. Therefore, it is crucial that a GMPE should properly estimate the seismic ground motion near the source fault. Most researchers use the term "far field" to refer to seismic ground motion far from the epicenter, but different names are used to describe the areas near the seismic source, such as near source, near fault, near field, or short hypocentral/epicentral distance. In this paper, the term "short distance" is used to refer to the area. Unlike the far field, the number of short-distance records is limited, and the empirical GMPE for the large earthquake in the short-distance region is based on relatively few observations.

Some studies that included close distances, such as Sadigh et al. [1997], presented attenuation relations for shallow earthquakes with magnitudes of 4 to 8 and rupture distances up to 100 km. Berge-Thierry et al. [2003], using European and US data, predicted ground motions for earthquakes larger than 4 with hypocentral distances between 4 and 330 km. Gok and Kaftan [2022] predicted peak ground acceleration using a neural network and IzmirNET strong motion network data with hypocentral distances between 10 and 400 km and magnitude Mw ≥ 4, focusing on shallow depths with distances of about 30 km. To derive a reliable GMPE for correct estimation at short distances, it is necessary to consider some characteristics, such as the ground motion saturation effect. According to Atkinson and Silva [2000], the ground motions can be correctly predicted at short distances using an effective distance metric (Eq. 1).

$$R = (D^2 + h^2)^{0.5} \tag{1}$$

where D is the closest distance (e.g., hypocentral or fault distance), and h is a pseudoterm that accounts for the distance-saturation effect. The saturation term depends on the magnitude, and for earthquakes with $M > 6$, it is modeled as Eq. (2) by Yenier and Atkinson [2014].

$$\log(h) = -1.72 + 0.43M \tag{2}$$

GMPEs are generally obtained by fitting a regression model to the ground motion dataset. Campbell and Bozorgnia [2003] have updated the near-source ground motion relations to extract a compatible set for horizontal and vertical ground motion relationships for peak ground acceleration and acceleration response spectra. They used globally recorded seismic data during shallow-crustal tectonic events at distances less than 60 km with magnitudes between 4.7 and 7.7.

Atkinson [2015] has developed a GMPE, Eq. (3) below, for small and moderate events with moment magnitudes from 3 to 6 at hypocentral distances less than 40 km and for a reference site condition corresponding to soft rocks.

$$\log Y = c_0 + c_1 M + c_2 M^2 + c_3 \log R, \tag{3}$$

and

$$R = \left(R_{\text{hyp}}^2 + h^2\right)^{0.5} \tag{4}$$

in which Y represents the median value of ground motion parameter, log is in base 10, M is moment magnitude, R_{hyp} is hypocentral distance. The distance saturation parameter, h, was set as Eq. (2) for $M > 4.0$.

The purpose of this study is to examine the effect of local site condition on the predictions of horizontal peak ground acceleration at very short hypocentral distances. For this purpose, we compare the regression models by adding predictors of average shear wave velocity at different depths of soil profile.

2. Data and Method

We used a dataset of accelerograms recorded in Japan by Kiban Kyoshin network (KiK-net). KiK-net consists of a pair of seismographs installed with the borehole and the earth's surface and is deployed to approximately 700 locations nationwide [NIED, 2019]. The dataset was selected from seismic records with magnitudes of 5.5 and higher recorded between 2000 and the end of 2023. The events included in the dataset had focal depths and epicentral distances of less than 20 km, as well as hypocentral distances of less than 25. The hypocentral distance range is defined based on the ratio between vertical and horizontal peak acceleration (V/H). The V/H relation shows a clear different behavior for distances less than 30 km from the source of earthquakes of M 5.5 to 7.5 [Elnashai and Papazoglou, 1997].

Despite the high seismicity of Japan and the large number of stations, only a very limited amount of data was collected due to the critical short hypocentral distances of less than 25 km. The collected data has been categorized into two sets: a regression set and a verification set. The regression set includes data from events that occurred between 2000 and 2018, while the verification set encompasses events between 2019 and 2023. For regression analysis, the dataset comprises 96 records with magnitudes ranging from 5.5 to 7.3. Among them, KiK-net provides

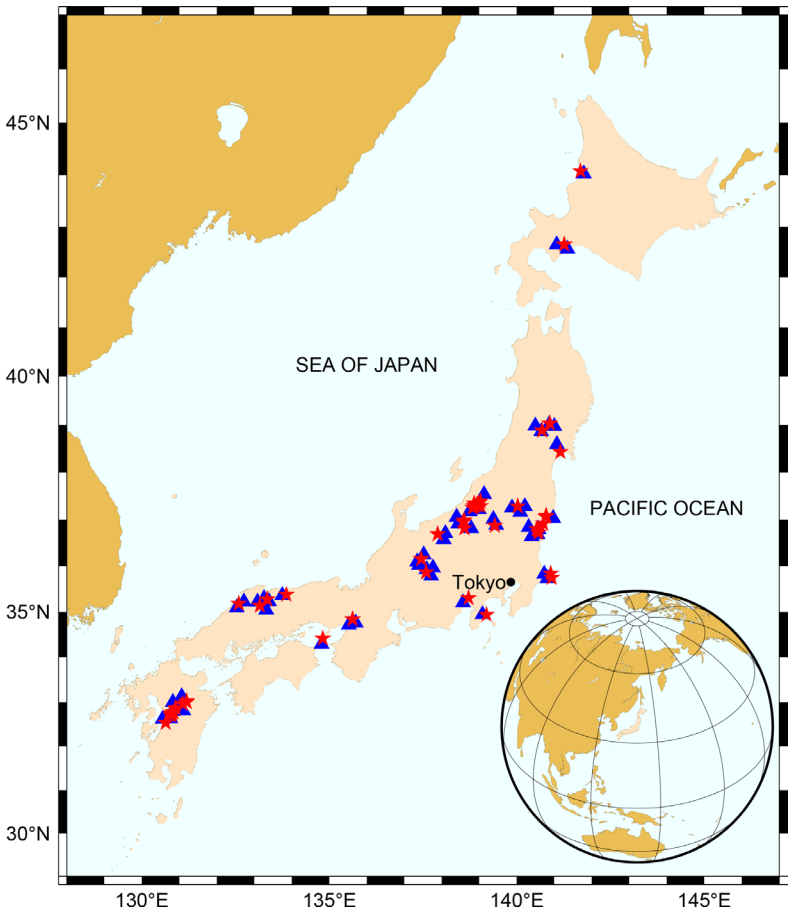

Figure 1. The distribution of earthquake epicenters (red stars) and KiK-net stations (blue triangles) used in this study. An inset in the bottom right corner shows the geographical location of Japan on the world map. The figure was generated using GMT, the Generic Mapping Tools software [Wessel and Smith, 1998].

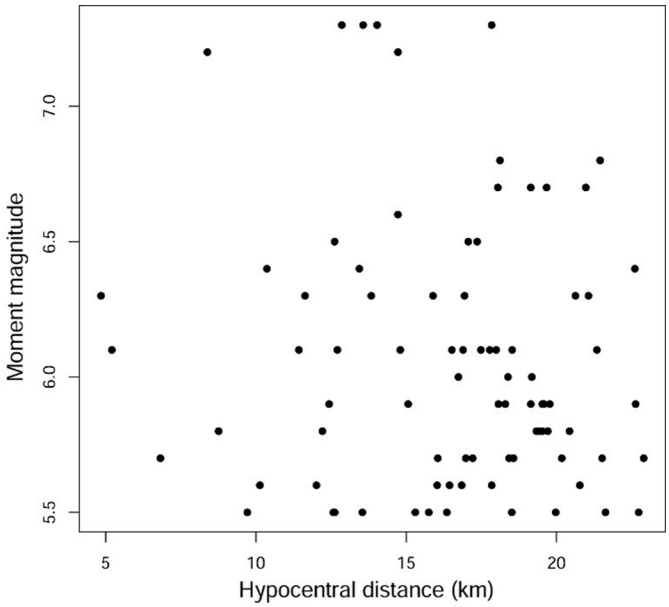

Figure 2. Moment magnitude and hypocentral distance distribution of PGA recordings used in this study.

a shear wave profile for the station site of 83 records. Figure 1 displays the epicentral distribution of earthquakes and the stations used in this study. The distribution of selected ground motion records with respect to magnitude and hypocentral distance is illustrated in Figure 2. Magnitudes mostly fall within the range of M 5.5 to 6.4. The hypocentral distance of the events ranged from 5 to 23 km; however, most events are in the range of 15 to 20 km. The largest events recorded were of magnitude 7.3. The regression technique utilized in this study is ordinary least squares (OLS). The statistical software R, by the R Core Team [2021], was employed for data analysis.

3. Regression Model and Results

We revised Atkinson's GMPE [2015] to investigate the effect of near-surface site conditions within the model as follows:

$$\log Y = c_0 + c_1 M + c_2 (M - \bar{M})^2 + c_3 \log R, \tag{5}$$

where Y represents the vector sum, i.e., the square root of the sum of squares of the peak horizontal components (NS and EW) in Gal units or cm/s^2, and it will be referred to as PGA hereafter. In the original equation, Eq. (3), the inclusion of the second power of M signifies that the amplitude behaves as a quadratic function of magnitude for hypocentral distances less than 40 km. This adjustment was made to depict the non-linear escalation of amplitudes with increasing magnitude at short distances. In the revised Equation, Eq. (5), the quadratic term is incorporated as $(M - \bar{M})^2$, where $\bar{M}$ represents the mean of the magnitude values. This change helps to mitigate the correlation between the first and second power terms of magnitude [Kutner et al., 2005]. Furthermore, the original model was specifically designed for a reference site condition with a near-surface shear-wave velocity of Vs30 = 760 m/s (where Vs30 represents the average shear wave velocity in the upper 30 meters). In this study, we utilized Eq. (5) across all site conditions. The estimated coefficients are summarized in Table 1, and the predicted attenuation curves for three different events are illustrated in Figure 3. The statistical properties presented in the table include the standard errors of the coefficients, p-values, and the R-squared correlation coefficient. Notably, the standard errors are less than half of the coefficient values. The p-values are mostly close to zero, indicating a significant relationship between the independent and dependent variables. With a correlation coefficient exceeding 0.6, we can conclude that the model passes statistical tests, allowing us to accept the model. In Figure 3, the PGA attenuation curves predicted for events of different magnitudes show the model's performance. These curves are paired with

observational data within the respective magnitude ranges, revealing a good fit between the predicted values and the observed data. Yenier and Atkinson [2014] have shown that the saturation of magnitude at very close distances led to peak accelerations lower than the expected values. Similarly, at distances less than 7 kilometers, we also observed a discrepancy between the magnitude and PGAs. To address this and adhere to the model's minimum distance limitation, Figure 3's graph starts at a hypocentral distance of 7 kilometers.

	C_0	C_1	C_2	C_3
Value	1.715	0.590	0.255	−2.281
Std. Error	0.472	0.077	0.099	0.293
P-value	0.000	0.000	0.012	0.000
No. of data = 83, Residual (RMS) = 0.244, $R^2 = 0.61$				

Table 1. Coefficients of Eq. (5) for all site conditions.

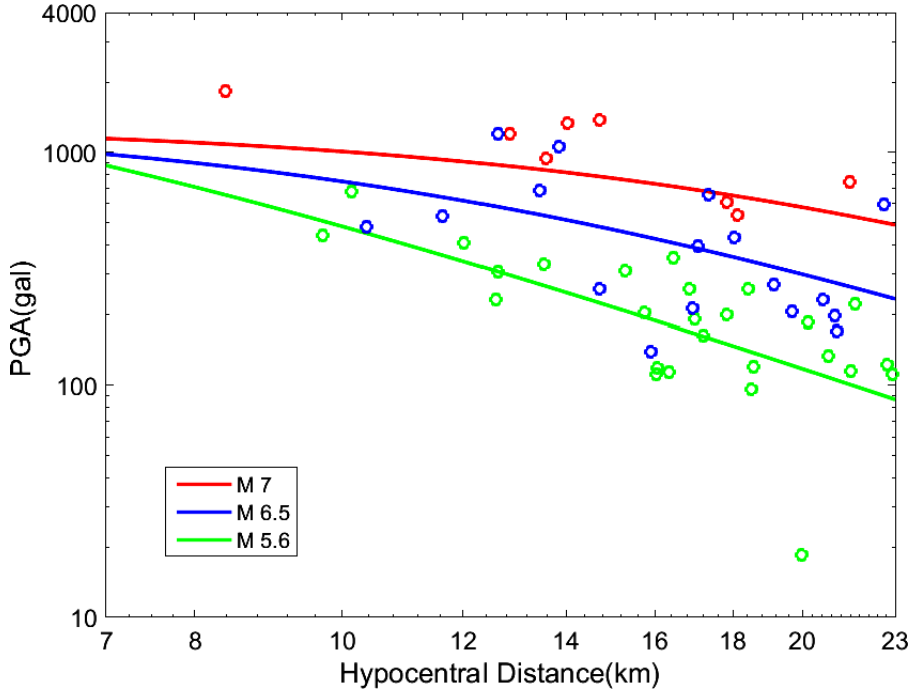

Figure 3. Predicted PGA attenuation curves for three different magnitudes. Each curve corresponds to magnitudes of 5.6, 6.5, and 7, distinguished by the colors green, blue, and red, respectively. The observed horizontal PGAs are indicated by colored-open circles and the assigned color is based on the magnitude closest to each of the three curves: the magnitude ranges from 5.5 to 5.7, 6.3 to 6.7, and 6.8 to 7.3, respectively.

The normality of the model residuals was evaluated by examining histograms and normal quantile-quantile (Q-Q) plots. Both the histogram and the Q-Q plot show an approximate normal distribution (Fig. 4). In Figure 5, a comparison of the results obtained from the proposed GMPE with those from Atkinson [2015] is presented. The curve derived from the proposed GMPE in this study (Eq. 5) aligns well with the observational data. However, the curve from Atkinson's GMPE [2015] (Eq. 3) shows a lower PGA prediction across all hypocentral distances.

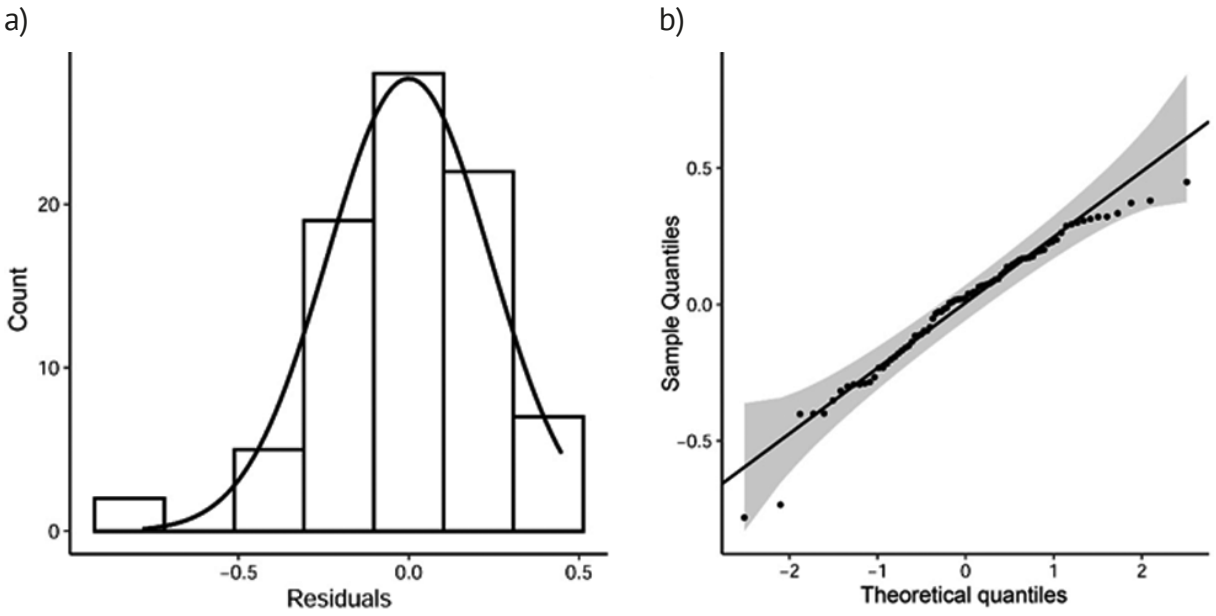

Figure 4. (a) Histogram of residuals with normal curve, and (b) Q-Q plot of residuals with 95% confidence band for Eq. (5).

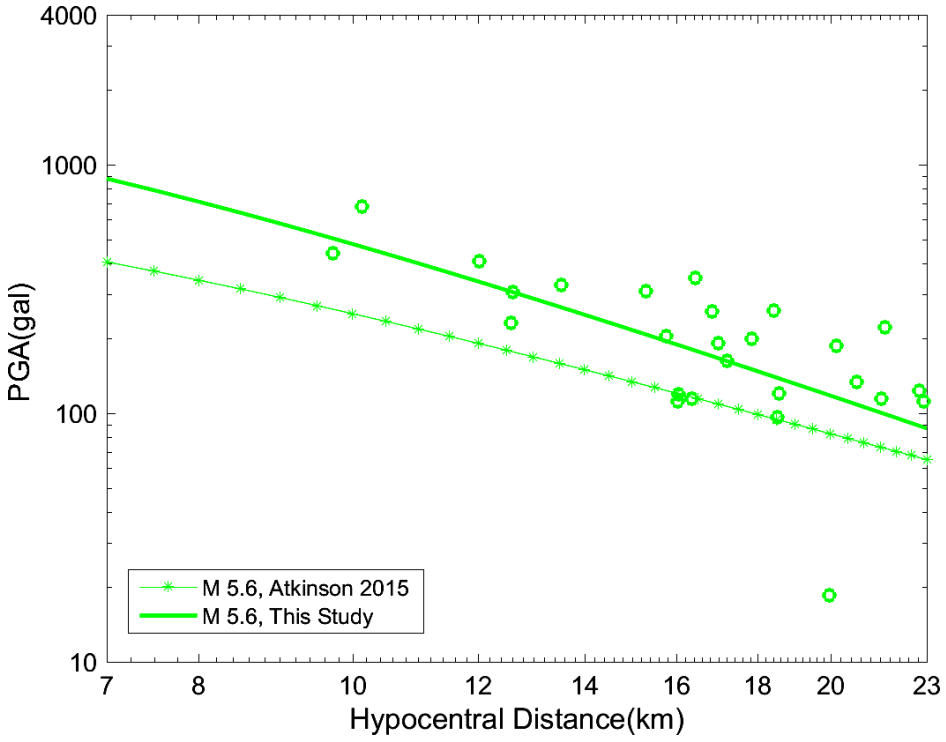

Figure 5. Comparison of the predicted PGA attenuation curves of Atkinson [2015] GMPE equation and the proposed equation. Observed PGAs for a magnitude range of 5.5 to 5.7 are shown with open circles.

To compare the results of our proposed model with previously studied models focusing on earthquakes in Japan, we consider two models: one by Chen et al. [2022] and the other by Kanno et al. [2006]. Chen et al. [2022] calculated the peak ground acceleration using the GMPE of Si and Midorikawa [1999], which takes into account the closest distance to a seismic fault. Meanwhile, Kanno et al. [2006] introduced their base model for shallow events to address amplitude saturation issues with decreasing source distance. The comparisons with Chen et al. [2022] and Kanno et al. [2006] can be observed in Figures 6 and 7, respectively. While these two models showcase a better

fit between observed and predicted PGAs compared to what is depicted in Figure 5, the former model in Figure 6 reveals a lower PGA prediction as hypocentral distances decrease, whereas the latter model in Figure 7 indicates an increased PGA prediction as earthquake magnitudes rise.

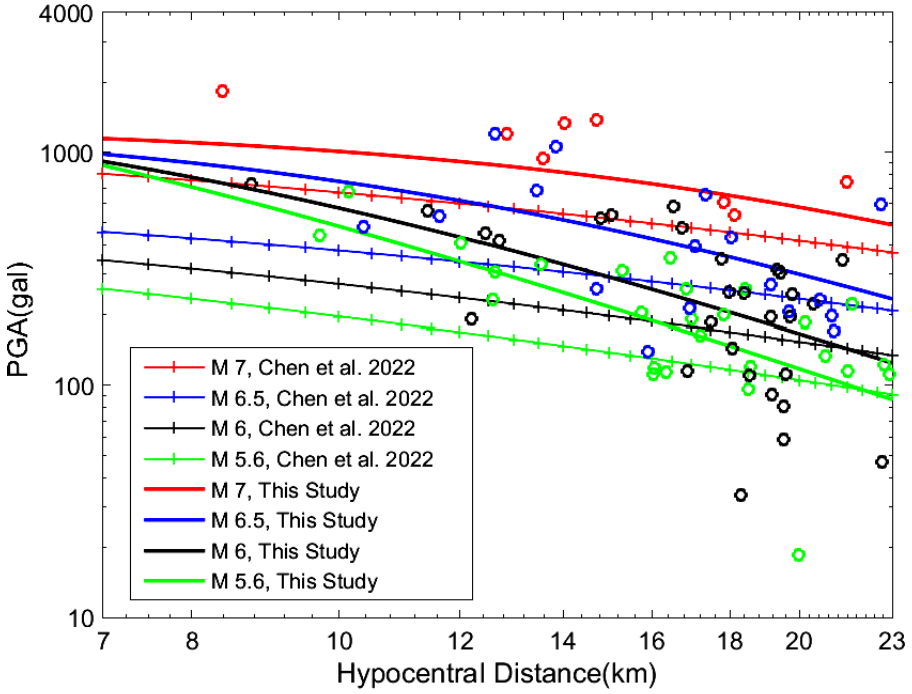

Figure 6. Comparison of the predicted PGA attenuation curves of Chen et al. [2022] GMPE and the proposed equation. The observed PGAs are indicated by colored-open circles, and the assigned color is based on the magnitude closest to each of the four curves: the magnitude ranges from 5.5 to 5.7, 5.8 to 6.2, 6.3 to 6.7, and 6.8 to 7.3, respectively.

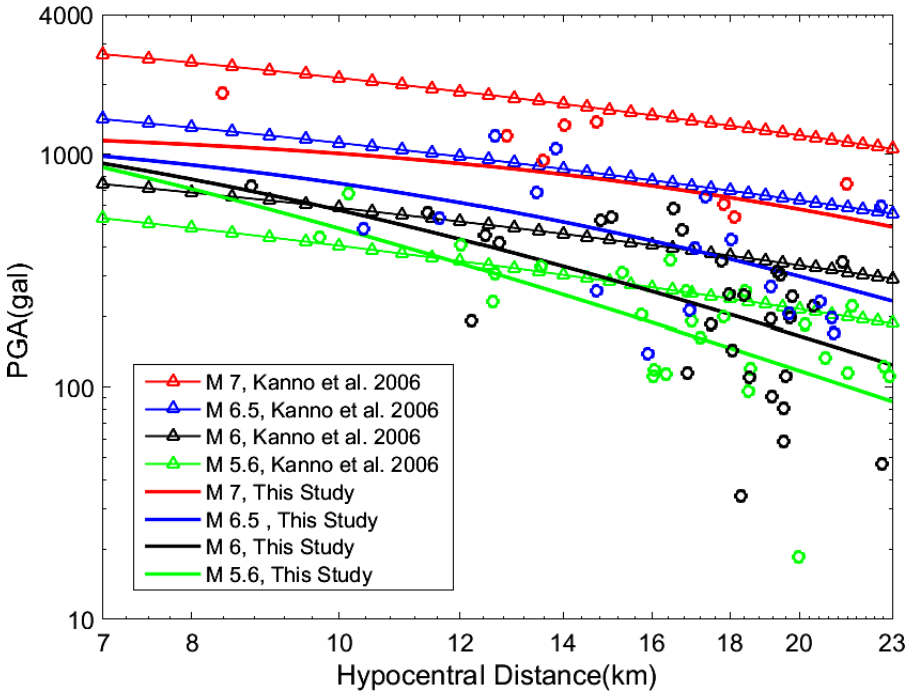

Figure 7. Comparison of the predicted PGA curves of Kanno et al. [2022] GMPE and the proposed equation. The observed PGAs are indicated by colored-open circles, and the assigned color is based on the magnitude closest to each of the four curves (see Fig. 6 for the range of the corresponding magnitude).

To validate our proposed model, we utilized a second dataset containing events between 2019 and 2023 that were not included in the initial regression analysis. Out of the 6 earthquakes recorded by K-NET stations, four of them were also recorded by KiK-net stations. For detailed information on the strong motion data, please refer to Tables 2 and 3. The regression model fitted to this dataset, indicating a reasonably good fit of the regression model, is presented in Figure 8.

Origin time	Station code	Latitude [N°]	Longitude [E°]	Epicentral Distance [km]	Depth [km]	Hypocentral Distance [km]	Magnitude	PGA [Gal]
18/06/2019 22:22	NIG006	38.61	139.48	17.375	14	22.313	6.7	315.521
18/06/2019 22:22	YMT004	38.61	139.48	9.757	14	17.064	6.7	852.426
13/03/2020 02:18	ISK003	37.28	136.82	14.766	12	19.027	5.5	297.286
13/03/2020 02:18	ISK005	37.28	136.82	8.885	12	14.932	5.5	310.092
13/03/2020 02:18	ISK006	37.28	136.82	17.630	12	21.326	5.5	123.934
13/03/2020 02:18	ISK015	37.28	136.82	9.504	12	15.308	5.5	529.332
23/04/2020 13:44	NGN013	36.23	137.66	13.238	3	13.574	5.5	91.986
23/04/2020 13:44	GIF004	36.23	137.66	11.997	3	12.366	5.5	170.148
18/03/2022 23:25	IWT003	39.99	142.00	9.963	18	20.573	5.6	371.225
05/05/2023 14:42	ISK001	37.54	137.3	11.913	12	16.909	6.5	589.107
05/05/2023 14:42	ISK002	37.54	137.3	10.175	12	15.733	6.5	728.782
05/05/2023 21:58	ISK001	37.52	137.24	5.845	14	15.171	5.9	675.735
05/05/2023 21:58	ISK002	37.52	137.24	9.812	14	17.096	5.9	447.774

Table 2. K-NET data for the years 2019 to 2023.

Origin time	Station code	Latitude [N°]	Longitude [E°]	Epicentral Distance [km]	Depth [km]	Hypocentral Distance [km]	Magnitude	PGA [Gal]
13/03/2020 02:18	ISKH04	37.278	136.823	13.505	12	18.066	5.5	189.870
23/04/2020 13:44	GIFH14	36.23	137.662	13.247	3	13.583	5.5	73.734
23/04/2020 13:44	NGNH30	36.23	137.662	18.020	3	18.268	5.5	84.389
05/05/2023 14:42	ISKH01	37.538	137.303	2.073	12	12.178	6.5	754.715
05/05/2023 21:58	ISKH01	37.525	137.235	4.360	14	14.663	5.9	534.553
05/05/2023 21:58	ISKH03	37.525	137.235	19.941	14	24.364	5.9	465.144

Table 3. KiKnet data for the years 2019 to 2023.

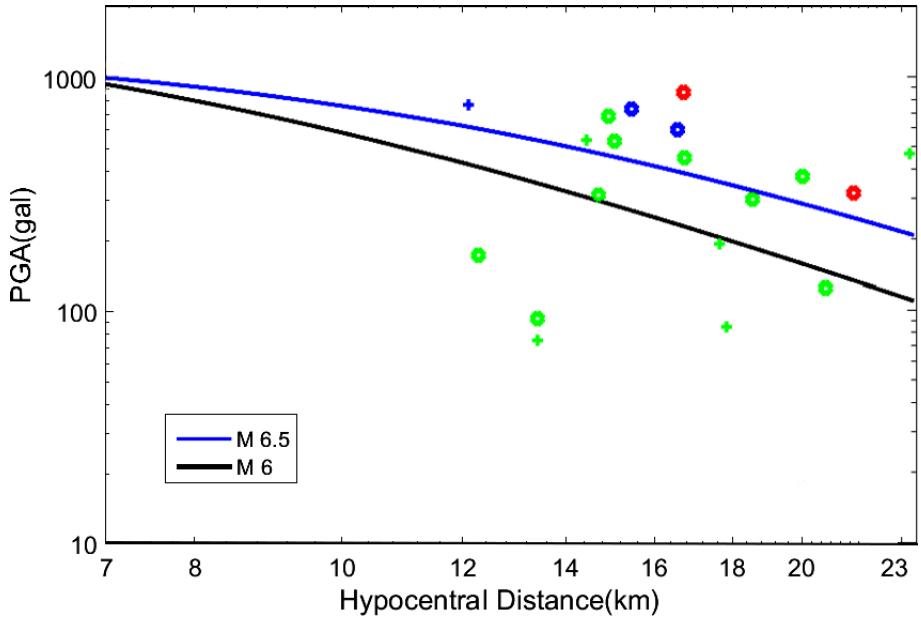

Figure 8. Predicted PGA attenuation curves for two different magnitudes along with observed PGAs from K-NET and KiK net for earthquakes that occurred between the years 2019 and 2023, which were not included in the regression analysis. The circle corresponds to K-NET data, and the plural sign corresponds to KiK net data. Green, blue, and red colors represent magnitude ranges of 5.5 to 6, 6 to 6.5, and 6.5 to 7, respectively.

For comparisons between different site conditions, the regression equation (i.e., Eq. 6) with an additional term, S, corresponding to the near-surface shear wave velocity is proposed.

$$\log \boldsymbol{Y} = \boldsymbol{c}_0 + \boldsymbol{c}_1\boldsymbol{M} + \boldsymbol{c}_2(\boldsymbol{M} - \bar{\boldsymbol{M}})^2 + \boldsymbol{c}_3 \log \boldsymbol{R} + \boldsymbol{c}_4\boldsymbol{S} \tag{6}$$

The most common classification for site condition is based on the Vs30 parameter. Some research has proposed a more cost-effective classification of sites with a shallower investigation depth [e.g. Gallipoli and Mucciarelli 2009; Boore 2004; Héloïse, et al. 2012]. In our study, regression analysis was performed with the site condition term defined by Vs30, along with the average shear wave velocities at shallower and more economical depths, specifically Vs20 and Vs15. The estimated coefficients along with their standard errors are detailed in Table 4. Importantly, the standard errors of the site condition term, C4, in all models are not less than half of their respective coefficient values. Figure 9 illustrates a forest plot for the visual comparison of estimated standardized model coefficients and confidence intervals, showing Eq. (5) for all sites and Eq. (6) for Vs30, Vs20, and Vs15 as site parameters. The figure demonstrates that the 95% confidence intervals of the site parameters intersect the line of no effect, suggesting that this parameter's impact on the estimation of horizontal vector peak ground acceleration at critically short hypocentral distances (< 23 km) is not statistically significant.

Model (Eq. 6)	C_0	C_1	C_2	C_3	C_4	R^2
forVs30	2.022 (0.500)	0.550 (0.080)	0.277 (0.099)	−2.239 (0.291)	−0.269 (0.159)	0.63
forVs20	1.988 (0.500)	0.550 (0.080)	0.276 (0.099)	−2.221 (0.293)	−0.294 (0.188)	0.62
for Vs15	1.997 (0.495)	0.542 (0.081)	0.283 (0.099)	−2.178 (0.296)	−0.380 (0.222)	0.63

Table 4. Coefficients of Eq. (6) with standard errors in parentheses for models incorporating near-surface shear wave velocity measurements (in km/s) at different depths: Vs30 (upper 30 meters), Vs20 (upper 20 meters), and Vs15 (upper 15 meters). Note that the number of data points used to fit each model was 83.

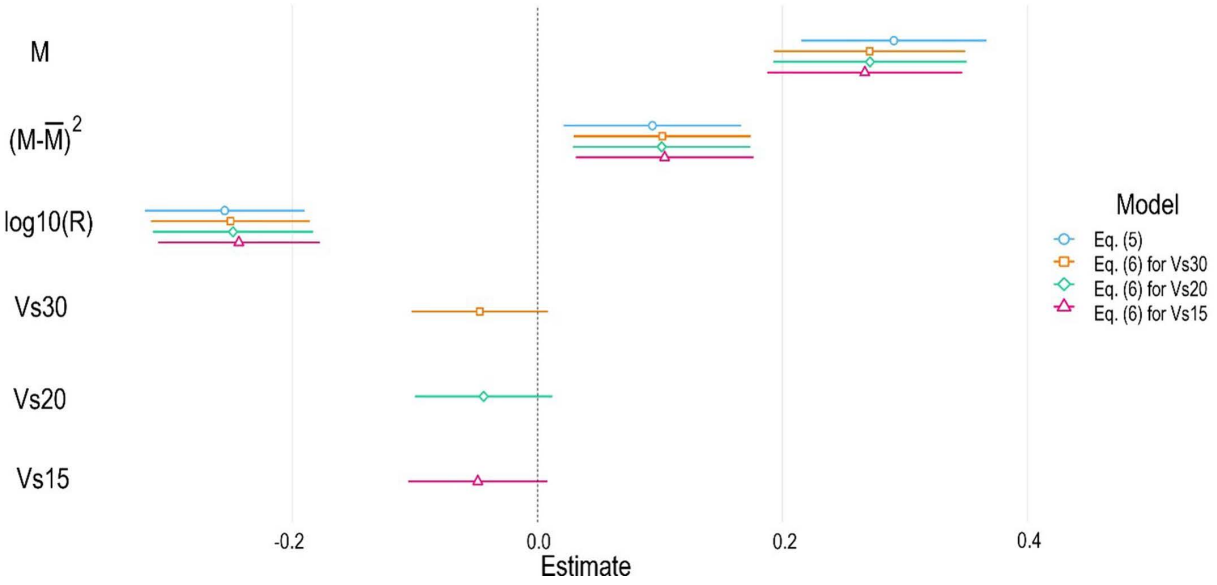

Figure 9. The forest plot illustrates the standardized coefficients along with their 95% confidence intervals for the examined models. The vertical dotted line represents a standardized coefficient of zero (line of no effect).

The dataset includes records from various faulting types displayed in Figure 10 through a ternary diagram of focal mechanisms, as described by Frohlich [1992]. The diversity of crustal faulting types and seismotectonic sources in different geological conditions suggests the potential wider implications of this study beyond the specific region. While generalizing these findings globally seems reasonable, further research with larger, more diverse datasets could enhance the robustness of our results and aid in improving seismic hazard assessment and risk mitigation strategies worldwide.

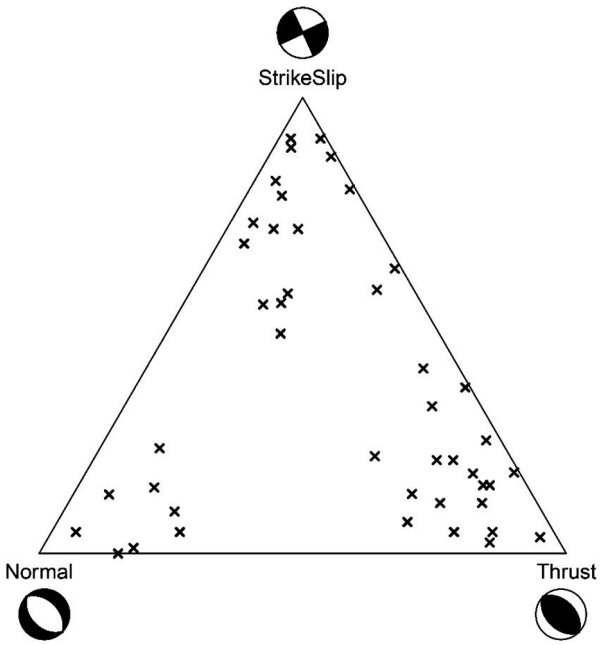

Figure 10. The diagram shows the distribution of event focal mechanisms with the three vertices representing pure strike-slip (top), pure normal fault (left), and a pure thrust fault (right). The space between these vertices defines the strike-slip, normal fault, and thrust fault groups.

4. Conclusions

In this study, we analyzed strong motion data from the KiK-net network in Japan to study horizontal vector peak ground accelerations (PGA) and their relation to site conditions at short hypocentral distances. Using seismic records from magnitude 5.5 and greater earthquakes between 2000 and 2023, we divided the data into regression and verification sets to develop and validate a revised regression model based on Atkinson's GMPE [2015]. Our study shows the revised model predicts PGAs well at short hypocentral distances. Comparing with other models, our proposed GMPE performs competitively in predicting ground motion characteristics, especially near seismic sources. We found that site conditions like Vs30, Vs20, and Vs15 did not significantly affect PGA estimations. Despite various crustal faulting types and seismotectonic sources in our dataset, more research with larger global datasets could enhance the applicability of our findings in seismic hazard assessment worldwide.

Data Availability Statement. The data used in this study is from the dataset K-NET, and KiK-net, provided by the National Research Institute for Earth Science and Disaster Resilience (NIED, 2019). The data is available to registered users at: https://www.kyoshin.bosai.go.jp/ (last accessed in June 2023).

Acknowledgements. The authors would like to thank the Editor and Reviewer of Annals of Geophysics Journal for their insightful comments, which significantly improved the manuscript. This research was funded by Ferdowsi University of Mashhad [Grant 3/50133].

References

Atkinson, G.M. and W. Silva (2000). Stochastic modeling of California ground motions, Bull. Seismol. Soc. Am., 90, 2, 255-274, https://doi.org/10.1785/0119990064.

Atkinson, G.M. (2015). Ground-motion prediction equation for small-to-moderate events at short hypocentral distances, with application to Induced-seismicity hazard, Bull. Seismol. Soc. Am., 105, 2A, 981-992, https://doi.org/10.1785/0120140142.

Berge-Thierry, C., F. Cotton, O. Scotti, D.A. Griot-Pommera and Y. Fukushima (2003). New empirical response spectral attenuation laws for moderate European earthquakes, J. Earthq. Eng., 7, 2, 193-222, https://doi.org/10.1080/13632460309350446.

Boore, D.M. (2004). Estimating VS10 (or NEHRP site classes) from shallow velocity models (Depths < 30 m), Bull. Seismol. Soc. Am., 94, 591-597, https://doi.org/10.1785/0120030105.

Campbell, K.W. and Y. Bozorgnia (2003). Updated near source ground-motion (attenuation) relations for the horizontal and vertical components of peak ground acceleration and acceleration response spectra, Bull. Seismol. Soc. Am., 93, 1, 314-331, https://doi.org/10.1785/0120020029.

Chen, W., D. Wang, H. Si and C. Zhang (2022). Rapid estimation of seismic intensities using a new algorithm that incorporates array technologies and ground-motion prediction equations (GMPEs), Bull. Seismol. Soc. Am., 112, 3, 1647-1661, https://doi.org/10.1785/0120210207.

Elnashai, S. and A.J. Papazoglou (1997). Procedure and spectra for analysis of RC structures subjected to strong vertical earthquake loads, J Earthq. Eng., 1, 1, 121-155, https://doi.org/10.1080/13632469708962364.

Fröhlich, C. (1992). Triangle diagrams: Ternary graphs to display similarity and diversity of earthquake focal mechanisms, Phys. Earth. Planet. Int., 75, 1, 193-198, https://doi.org/10.1016/0031-9201(92)90130-N.

Gallipoli, M.R. and M. Mucciarelli (2009). Comparison of site classification from VS30, VS10, and HVSR in Italy, Bull. Seismol. Soc. Am., 99, 340-351, https://doi.org/10.1785/0120080083.

Gök, E. and I. Kaftan (2022). Prediction of Peak Ground Acceleration by Artificial Neural Network and Adaptive Neuro-fuzzy Inference System, Ann. Geophys., 65, 1, SE106, https://doi.org/10.4401/ag-8659.

Héloïse, C., P.Y. Bard, A.M. Duval and E. Bertrand (2012). Site effect assessment using KiK-net data: part 2-site amplification prediction equation based on f0 and Vsz, Bull. Earthquake Eng., 10, 451-489, https://doi.org/10.1007/s10518-011-9298-7.

Kanno, T., A. Narita, N. Morikawa, H. Fujiwara and Y. Fukushima (2006). A New Attenuation Relation for Strong Ground Motion in Japan Based on Recorded Data, Bull. Seismol. Soc. Am., 879-897, https://doi.org/10.1785/0120050138.

Kutner, H.M., Ch.J. Nachtsheim, J. Neter and W. Li (2005). Applied Linear Statistical Models, McGraw-Hill/Irwin, New York, NY, USA.

NIED (2019). National Research Institute for Earth Science and Disaster Resilience (NIED) K-NET, KiK-net, Natl. Res. Inst. Earth Sci. Disaster Resil, https://doi.org/10.17598/NIED.0004.

Ohno, S., T. Ohta, T. Ikeura and M. Takemura (1993). Revision of attenuation formula considering the effect of fault size to evaluate strong motion spectra in near field, Tectonophysics, 218, 69-81, https://doi.org/10.1016/0040-1951(93)90260-Q.

R Core Team (2021). R: A language and environment for statistical computing, Vienna, Austria, https://www.R-project.org/ Accessed 7 August 2021.

Sadigh, K.C., Y. Chang, J.A. Egan, F. Makdisi and R.R. Youngs (1997). Attenuation relationships for shallow crustal earthquakes based on California strong motion data, Seism. Res. Lett., 68, 1, 180-189, https://doi.org/10.1785/gssrl.68.1.180.

Si, H.J. and S. Midorikawa (1999). New attenuation relationships for peak ground acceleration and velocity considering effects of fault type and site condition, J. Struct. Constr. Eng., 523 63-70, https://doi.org/10.3130/aijs.64.63_2 (in Japanese with English abstract).

Wessel, P. and W.H.F. Smith (1998). New improved version of generic mapping tools released, EOS Trans. AGU, 79, 579, https://doi.org/10.1029/98EO00426.

Yenier, E. and G.M. Atkinson (2014). Equivalent point-source modeling of moderate to large magnitude earthquakes and associated ground motion saturation effects, Bull. Seismol. Soc. Am., 104, 3, 1458-1478, https://doi.org/10.1785/0120130147.

***CORRESPONDING AUTHOR: Hossein SADEGHI**
Ferdowsi University of Mashhad, Azadi Square, 9177948974, Mashhad, Iran
e-mail: sadeghi@um.ac.ir